# Kinetic Modeling of Transient Photoluminescence from Thermally Activated Delayed Fluorescence

Nils Haase,[*,†,‡] Andrew Danos,[*,§] Christof Pflumm,[‡] Antonia Morherr,[‡] Patrycja Stachelek,[§] Amel Mekic,[‡,∥] Wolfgang Brütting,[†] and Andrew P. Monkman[§]

[†]Institute of Physics, Experimental Physics IV, University of Augsburg, Universitätsstr. 1, 86135 Augsburg, Germany
[‡]Merck KGaA, Performance Materials - Display Solutions, Frankfurter Straße 250, 64293 Darmstadt, Germany
[§]Department of Physics, Durham University, South Road, Durham DH1 3LE, United Kingfom
[∥]Institute of Organic Chemistry, University of Regensburg, Universitätsstr. 31, 93053 Regensburg, Germany

## INTRODUCTION

In contrast to phosphorescent iridium or triplet−triplet annihilation (TTA) based organic light emitting diodes (OLEDs), devices that harvest triplet excitons using thermally activated delayed fluorescence (TADF) promise to deliver deep blue emission and internal quantum efficiencies (IQE) up to 100% while also avoiding the use of precious metals.[1−9] TADF materials rely on a small energy splitting between the lowest excited singlet and triplet states ($\Delta E_{ST}$), such that thermally activated reverse intersystem crossing (rISC) can promote the upconversion of nonemissive triplet states.

While considerable work has been done to design highly efficient TADF molecules with a small $\Delta E_{ST}$, examples of poor TADF compounds with very low $\Delta E_{ST}$ demonstrate that it is not the only relevant design factor.[10] Instead, the true criterion for efficient TADF is simply a large rISC rate constant ($k_{rISC}$). Despite this central importance, no practical yet theoretically sound method for the determination of $k_{rISC}$ as part of the routine characterization of TADF materials has been provided - until now.

Unfortunately, a direct measurement of $k_{rISC}$ is difficult and requires complex modeling of ultrafast transient absorption.[11] Nonetheless, various indirect approaches exist to describe the kinetic behavior of TADF molecules and obtain approximate values of $k_{rISC}$. Early on, TADF materials were described in terms of the equilibrium model.[12,13] More recently, Dias et al.[14] estimated $k_{rISC}$ from the photoluminescence quantum yields (PLQY) and exponential lifetimes of the prompt fluorescence and the delayed fluorescence via

$$k_{rISC} = \frac{1}{\tau_{DF}} \frac{\Phi_{PF} + \Phi_{DF}}{\Phi_{PF}} = \frac{1}{\tau_{DF}} \left(1 + \frac{I_{DF}}{I_{PF}}\right) \quad (1)$$

where $\tau_{DF}$ is the lifetime of the delayed fluorescence, $\Phi_{PF}$ is the photoluminescence quantum yield of the prompt fluorescence, and $\Phi_{DF}$ the photoluminescence quantum yield of the delayed fluorescence. This can also be expressed in terms of $I_{DF}/I_{PF}$, the ratio of total emission signal from delayed and prompt emission. In deriving eq 1, the assumption is made that nonradiative processes from the triplet state are suppressed such that $\Phi_{rISC} \approx 1$, which is ensured when $\Phi_{DF}/\Phi_{PF} \gtrsim 4$.[14]

Two experimental approaches exist to evaluate eq 1, although neither can be universally applied. Common to both methods, time-resolved emission measurements must be made and exponential fitting performed to determine $\tau_{DF}$. While this process is often straightforward, identifying the appropriate time region for fitting can be challenging in solid hosts, where an ensemble of TADF molecular geometries and microenvironments can result in complex multiexponential decay in the delayed regime.[15] This is especially the case at low temperatures, where phosphorescence emission can compete with inhibited TADF. Exponential fitting is then also applied in

the prompt region, allowing $I_{DF}/I_{PF}$ to be evaluated as the ratio of areas bound by the fitted exponential curves in the delayed and prompt regions.

Alternatively, steady state measurements can be compared in air and inert atmosphere. By assuming that oxygen fully quenches all triplet states and thus any delayed emission, the ratio $(\Phi_{PF} + \Phi_{DF})/\Phi_{PF}$ can be replaced by the ratio of PLQYs or total emission intensities in vacuum (PF and DF), and in air (PF only). This assumption does not hold in all circumstances though, as high performance TADF materials may have rISC rates large enough to compete with oxygen quenching, while some hosts can restrict oxygen diffusion and its ability to quench triplets in a solid film. Any additional $\Phi_{DF}$ contribution to the oxygenated measurement results in an underestimate of $k_{rISC}$, and is exacerbated when $k_{rISC}$ is already large.

Although applied successfully elsewhere,[14,16] both methods of evaluating eq 1 ultimately rely on partitioning the emission decay kinetics into prompt and delayed regions for fitting. While Adachi and co-workers have recently reported three and four level TADF models that indeed have exponential analytic solutions, the interaction of population dependent emission, ISC, and rISC rates means that the fitted exponential prefactors and decay rates are highly interlinked. In this framework eq 1 is revealed to lack a sound theoretical basis and is at best an approximation (albeit a very useful and successful one). Instead, challenging algebra is required to relate the fitting parameters of these analytic solutions to the rate constants of interest, which limits the practicality of this approach. Focusing only on the most delayed rate constant can simplify analysis, but at the cost of discarding any fitting power available through the prompt decay data. We also reiterate that in practice it is rarely possible to unambiguously identify separate regions for exponential fitting in the first place, a prerequisite for any analytic approach.[17,18]

In contrast to the approaches above, Penfold et al. recently considered the TADF mechanism as a kinetic process, which allows rapid extraction not only of rate constants but also time dependent state populations from transient photoluminescence experiments.[19] Here, we apply this model to obtain values of $k_{rISC}$ and other key rate constants from time-resolved photoluminescence measurements of two high performance D-A-D TADF materials. Additionally, applying the kinetic model to data taken at different temperatures allows us to determine the activation energies of TADF in these materials, which are in close agreement with previously determined values.

(It is instructive to note the parallel development of TADF and TTA research, both of which involve prompt and delayed emission components that can be modeled with biexponential decays. For TTA, the fast and slow processes correspond to second and first order decay mechanisms operating on the same triplet population. Differential equations (some with convenient analytic solutions) have widely replaced the use of exponential fitting for TTA, enabling the annihilation rate constant to be reliably determined.[17,18] Here we apply similar methods to TADF.)

## METHODS AND KINETIC MODEL

In photoluminescence experiments, there are usually two channels to optically excite a D−A or D−A−D TADF molecule. Excitons can be generated on a local excited singlet state ($^1$LE) via a strong local donor (or acceptor) $\pi$−$\pi$* transition,[20] which can then either decay radiatively or undergo electron transfer to form a singlet charge transfer state ($^1$CT). Alternatively, the $^1$CT state can be excited directly through a weak (n−$\pi$*/ $\pi$−$\pi$*) mixed transition.[14] Since both $^1$LE and $^1$CT have fast radiative decay rates, simultaneous emission typically occurs for the first ∼5 ns.[14] For later times the $^1$LE contribution to the emission spectra vanishes while $^1$CT emission persists as the $^1$CT state is continually repopulated by TADF. Therefore, only one singlet state ($S_1$) is directly considered in the simplified rate model presented here (shown in the right of Figure 1). To evaluate the contribution of the $^1$LE emission at early times the initial population of the singlet state $[S_1](t = 0)$ is taken as an additional fit parameter.

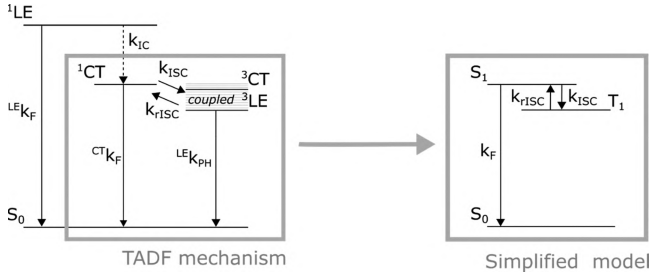


**Figure 1.** Left: Schematic representation of the energy levels and rate constants that govern TADF kinetics. Right: Simplified model used to extract rate constants and state populations.

The TADF mechanism itself is based on a complex four-state model, shown in the left gray box of Figure 1, where the $^1$CT, $^3$CT, and $^3$LE states are mixed through a second order coupling.[21−24] Once the excited $^1$CT state is formed it can either decay radiatively yielding prompt $^1$CT fluorescence emission, or it can populate the $^3$LE state via intersystem crossing (ISC). Both nonadiabatic coupling and thermal energy then lead to mixing and formation of equilibrium populations in $^3$CT and $^3$LE, at rates far exceeding that of spin−orbit coupling (SOC) between the $^1$CT and $^3$LE state.[22,25] Indeed, calculations by Gibson and Penfold show that the equilibrium between $^3$CT and $^3$LE is only very weakly temperature dependent[25] and that for small energy gaps between those two states the nonadiabatic vibronic coupling is strong enough to populate the $^3$CT state even at 0 K. Consequently, we consider only one mixed triplet state ($T_1$) as the lowest lying triplet state in the simplified TADF model. Slow phosphorescence and nonradiative pathways are not considered in this model, justified by transient absorption measurements presented further below. As is necessary in deriving eq 1, this is equivalent to assuming $\Phi_{rISC} \approx 1$.

The simplified model of the TADF process forms a system of linear differential equations:

$$\frac{d[S_1]}{dt} = -(k_F + k_{ISC})[S_1] + k_{rISC}[T_1] \quad (2)$$

$$\frac{d[T_1]}{dt} = k_{ISC}[S_1] - k_{rISC}[T_1] \quad (3)$$

The time-dependent rate model is solved numerically using the odeint function from the SciPy library in Python 3.6 for specific values of $k_F$, $k_{ISC}$, $k_{rISC}$ and $[S_1](t = 0)$, with $[T_1](t = 0)$ set to zero. To extract the rate constants and state population kinetics, we fit $[S_1]$ to normalized data of transient photoluminescence experiments using the curve_fit tool from SciPy. Since $S_1$ is the only emissive state in the considered model, its

population is directly proportional to the photoluminescence emission intensity. The implementation of this fitting model is presented in detail in the Supporting Information, with particular attention given to methods of parameter optimization and sensitivity to starting values.

## RESULTS AND DISCUSSION

Using the kinetic model discussed above, we analyzed the kinetics of the D−A−D TADF molecules DDMA-TXO2[26,27] and DPTZ-DBTO2[14] in solid state. Both emitters show clear delayed emission and give excellent device performances with maximum external quantum efficiencies (EQE) above 18%. Figure 2 shows the emission decay from the early prompt emission to the end of the delayed fluorescence of DPEPO:DDMA-TXO2(13 vol % emitter in host) at 290 K taken from ref 26 and CBP:DPTZ-DBTO2(10%) at 298 K taken from ref 14. In addition, the fitted time dependent singlet and calculated triplet populations are shown, and are found to accurately reproduce independent transient absorption measurements presented in Figure 5. The best fit results obtained are shown in Table 1.

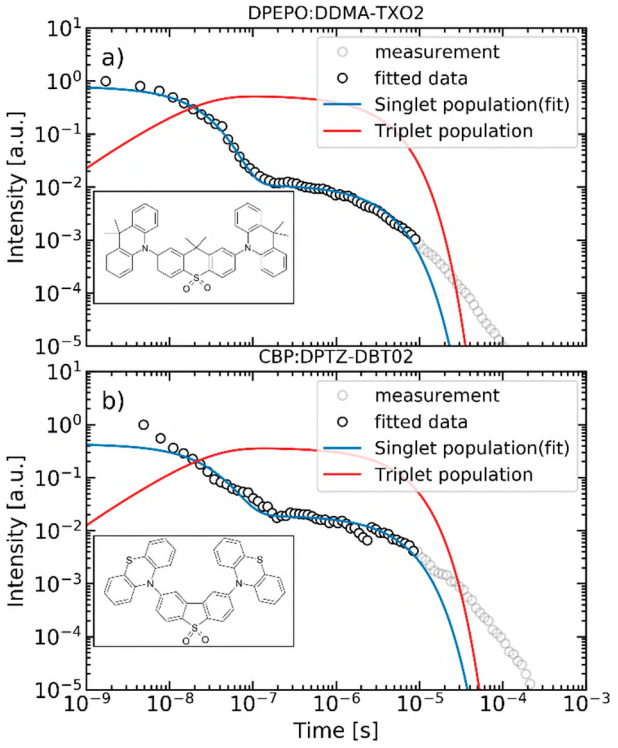


**Figure 2.** Structures (inset) and emission decay (black circles) of (a) DPEPO:DDMA-TXO2(13%)[26] and (b) CBP:DPTZ-DBTO2(10%)[14] at room temperature. Also shown are the fitted time dependent singlet (blue) and calculated triplet populations (red) for each emitter. Gray data points are not included in the fits shown, but are found to have negligible influence on the final fit parameters as discussed in the Supporting Information.

For both materials the singlet population accurately describes the emission decay for several orders of magnitude and shows clear prompt and delayed contributions. The singlet population is not in good agreement with the recorded emission only at very early and very late times. At very early times the emission is a combination of fluorescence from $^1$CT and $^1$LE.[14] Supporting this, Figure 3 shows an additional contribution to the total emission in the spectra for both samples at early times, presumably from the $^1$LE emission of the donor unit. For DPEPO:DDMA-TXO2(13%) the $^1$CT emission is already dominant at 3.5 ns, while the major contributor to emission for CBP:DPTZ-DBTO2(10%) is the $^1$LE state until at least 7.8 ns. This observation is consistent with the fit values of $[S_1](t = 0)$, 78.4% for DPEPO:DDMA-TXO2(13%) and 43.1% for CBP:DPTZ-DBTO2(10%), which represent the proportion of the initial total emission intensity that originates from the $^1$CT state. After about 18 ns, the $^1$LE contribution to the emission spectra vanishes for both materials, and the kinetic model begins to accurately describe the experiment.

The additional emission at very late times can be attributed to long living but weak emission from a small subset of molecules which cannot undergo rapid rISC due to unfavorable D−A angles.[14] An ensemble of different D−A angles is expected to give rise to an ensemble of $k_{rISC}$ values and the resulting power law behavior (appearing linear on a log−log scale). As the validity of the kinetic modeling is concerned, we note that the overall intensity in this regime is exaggerated by the log−log figure axes, and is both relatively and absolutely small. Furthermore, we also find that the fitted rate constants are insensitive to the inclusion or exclusion of this tail region, as detailed in the Supporting Information. Nonetheless, a decisive advantage of our kinetic approach compared to existing ones is that eq 3 can be readily modified or expanded to treat an ensemble of rISC rates as needed in future.

Figure 4 shows the temperature dependence of emission decays from the films of DPEPO:DDMA-TXO2(13%) and CBP:DPTZ-DBTO2(10%) (taken from refs 26 and 14)

**Table 1. Fitted Rate Constants, and $k_{rISC}$ Values Determined Using Dias Method**

| DPEPO:DDMA-TXO2(13%) | | | | | |
|---|---|---|---|---|---|
| $T$ [K] | $[S_1](t = 0)$ [%] | $k_F$ [$10^6$ s$^{-1}$] | $k_{ISC}$ [$10^6$ s$^{-1}$] | $k_{rISC}$ [$10^5$ s$^{-1}$] | $k_{rISC}$ [$10^5$ s$^{-1}$] by Dias et al.[14] |
| 290 | 78.4 ± 0.1 | 15.0 ± 0.3 | 32.4 ± 1.2 | 9.8 ± 0.3 | 10.8 |
| 230 | 83.6 ± 5.5 | 14.4 ± 0.8 | 31.5 ± 1.2 | 9.3 ± 0.4 | 10.0 |
| 180 | 80.6 ± 5.6 | 18.4 ± 1.0 | 26.7 ± 1.0 | 7.1 ± 0.3 | 8.0 |
| 130 | 78.3 ± 4.6 | 26.0 ± 1.1 | 20.6 ± 0.7 | 4.9 ± 0.2 | 5.4 |
| CBP:DPTZ-DBTO2(10%) | | | | | |
| $T$ [K] | $[S_1](t = 0)$ [%] | $k_F$ [$10^6$ s$^{-1}$] | $k_{ISC}$ [$10^6$ s$^{-1}$] | $k_{rISC}$ [$10^5$ s$^{-1}$] | $k_{rISC}$ [$10^5$ s$^{-1}$] by Dias et al.[14] |
| 298 | 43.1 ± 5.1 | 4.0 ± 0.5 | 33.4 ± 3.2 | 19.3 ± 2.0 | 18.1 |
| 220 | 40.7 ± 4.1 | 6.1 ± 0.7 | 34.3 ± 2.4 | 12.6 ± 1.0 | 12.9 |
| 160 | 44.1 ± 3.6 | 8.8 ± 0.9 | 20.7 ± 1.1 | 4.1 ± 0.3 | 4.6 |

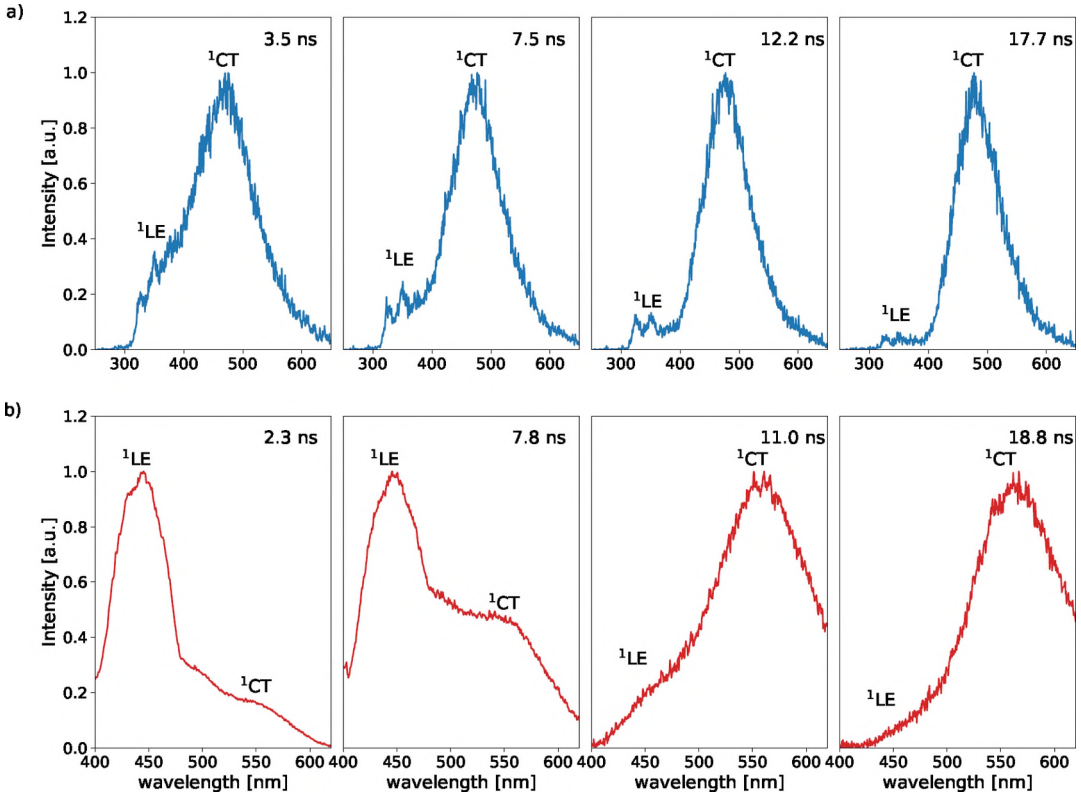


**Figure 3.** Time resolved emission spectra of (a) DPEPO:DDMA-TXO2(13%) and (b) CBP:DPTZ-DBTO2(10%), obtained at very early times following the excitation.

together with the fitted singlet population. The changes with temperatures for DPEPO:DDMA-TXO2(13%) are relatively small compared to the CBP:DPTZ-DBTO2(10%) sample, qualitatively indicative of a smaller energy gap for DPEPO:DDMA-TXO2(13%). The best fit results obtained for the different temperatures and TADF emitters are shown in Table 1. For all photoluminescence decays, the singlet population follows the experimental data over several orders of magnitude. Only at very early (<20 ns) and very late times (>10 $\mu$s), does the fit not describe the emission accurately, as discussed above. The values of $k_{rISC}$ also compare well to those determined using eq 1 ($I_{DF}/I_{PF}$ via areas method) for all evaluated temperatures, without requiring selection of segregated prompt and delayed regions. As the values for $k_{rISC}$ are faithfully reproduced by our method, estimates of $\Delta E_{ST}$ derived from the changes in $k_{rISC}$ with temperature will also agree with existing methods based on eq 1.

We also find that $k_{ISC}$ increases with increasing temperature in a similar fashion to $k_{rISC}$. In contrast, $k_F$ is found to decrease with increasing temperature for both materials. This decrease cannot be the result of an unmodeled temperature dependent increase of nonradiative rate constants, as the PLQY of DPEPO:DDMA-TXO2(13%) at room temperature is as high as 95 ± 5%.[26] To explain this trend, we suggest that the average D−A dihedral angle is temperature dependent and shifts closer to orthogonality at higher temperatures. This change in geometry reduces the overlap between donor and acceptor groups, leading to the observed increase in $k_{ISC}$ and reduction in $k_F$.[15]

The initial state population $[S_1](t = 0)$ shows no temperature dependence for either sample, with values consistently higher for DPEPO:DDMA-TXO2(13%) compared to CBP:DPTZ-DBTO2(10%). This difference reflects the larger initial contribution of $^1$LE to the emission of the CBP:DPTZ-DBTO2(10%) film (Figure 3), determined by both the competition of rates for $^1$LE emission and electron transfer (to form CT states), as well as the ratio of $^1$LE and direct $^1$CT absorption using 355 nm excitation. Neither of these factors are expected to be temperature sensitive. Instead we find that the fitted value of $[S_1](t = 0)$ is highly sensitive to the selection of the initial data point for normalization, in both materials rising to 100% when chosen at times after $^1$LE emission increases. Indeed, while we employ $[S_1](t = 0)$ as a fitting parameter here, alternate future implementations may instead set its value by careful comparison of $^1$CT and $^1$LE intensities in the earliest spectrum of a decay series (for molecules where these emissions are easily resolvable). We also find improved fitting at early times if only the wavelengths corresponding to $^1$CT emission are integrated to generate decay curves.

The values of $k_{rISC}$ are found to display Arrhenius-like behavior as shown in Figure 4c, the gradient of which is used to determine the activation energy of rISC. We obtain an activation energy of (14 ± 1) meV for the DPEPO:DDMA-TXO2(13%) and (47 ± 3) meV for the CBP:DPTZ-DBTO2(10%) sample, respectively, analogous to Arrhenius analysis of delayed emission intensity employed by others.[8,14,25] These values are close to those determined from the optical energy gap $\Delta E_{ST}$ calculated from the energy difference between the onset of the $^1$CT and $^3$LE emission as described elsewhere,[26] which are reported as (10 ± 3) meV for DPEPO:DDMA-TXO2(13%) and (20 ± 4) meV for CBP:DPTZ-DBTO2(10%),[14,26] respectively. Since the activation energy and the energy gap extracted from the emission

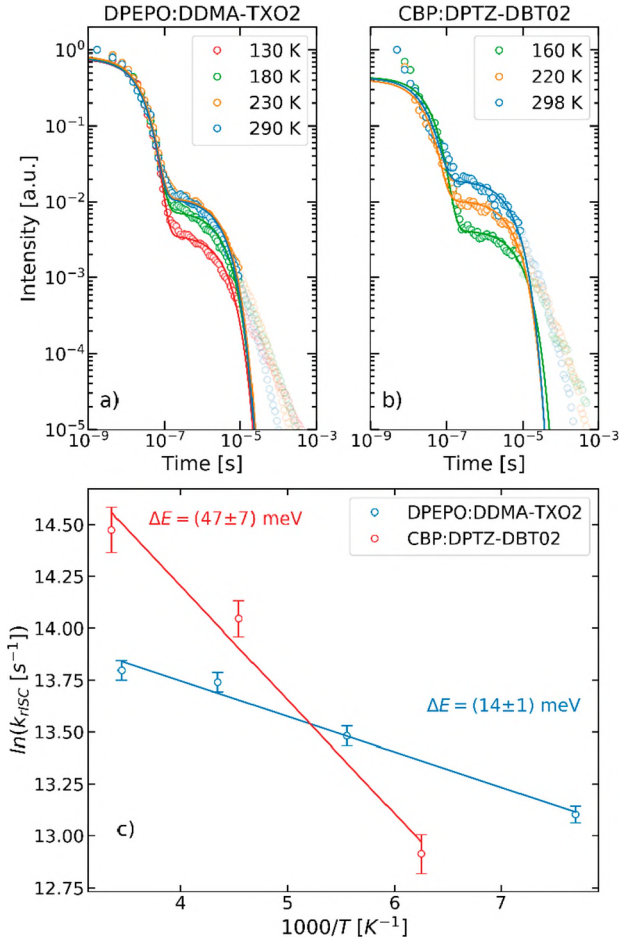


**Figure 4.** (a,b) Emission decay of DPEPO:DDMA-TXO2(13%) and CBP:DPTZ-DBTO2(10%), as a function of temperature (circles), together with the fitted singlet population (lines). (c) Arrhenius plot of $k_{rISC}$ values fitted from the decays. Gray data points are not included in the fits shown.

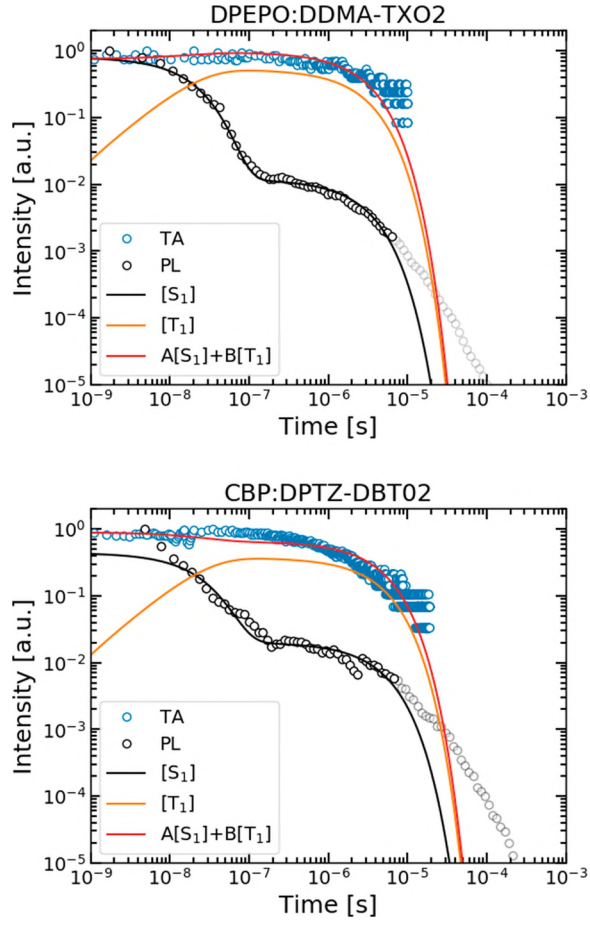


**Figure 5.** Transient absorption data (TA), along with independently measured and fitted emission (PL) decay. Linear combinations of the singlet and triplet populations from fitted photoluminescence decays ($A[S_1] + B[T_1]$) are able to accurately reproduce the experimental absorption data.

onset describe the energy difference between different states of the TADF process, it has been repeatedly found that the calculated energy gap differs between these approaches, especially for better performing molecules.[3]

Finally, we reiterate that the approach above does not consider any triplet decay (radiative or nonradiative), as justified at first by absence of phosphorescence spectra in the decays and the quality of subsequent fits. Independent justification for this approach is given by transient absorption (TA) measurements of both materials at room temperature shown in Figure 5 (blue circles). Also included are the emission decay data with triplet and singlet populations from fitting (identical to Figure 2). Descriptions of the sample preparation, TA apparatus, and data processing are included in the Supporting Information. Strong and long-lived TA signal consistent with photogenerated triplet states were observed at 600 nm for DPEPO:DDMA-TXO2(20%) and 650 nm for CBP:DPTZ-DBTO2(20%).

We find that the TA data can be reproduced from a linear combination of the triplet and singlet populations generated only from the PL decay. The best fits are shown as red lines in Figure 5, and come from $0.89[S_1] + 0.59[T_1]$ for DPEPO:DDMA-TXO2(20%) and $0.75[S_1] + 0.9[T_1]$ for CBP:DPTZ-DBTO2(20%), although these values are somewhat meaningless as all populations and the TA data itself are individually normalized.

We interpret the fact that the TA signal can be fit using linear combinations of $[S_1]$ and $[T_1]$ as evidence that it consists of contributions from short-lived $S_1 \rightarrow S_n$ and long-lived $T_1 \rightarrow T_n$ transitions. Critically, the good agreement of the TA data at long times (coming from triplet absorptions) with the $[T_1]$ population from emission decay fitting demonstrates that the fitted $[T_1]$ accurately describe the actual triplet population kinetics in the material. Since the fitted $[T_1]$ curves are generated without inclusion of kinetic terms for triplet radiative or nonradiative decay, the agreement with TA measurements confirms that these processes are indeed negligible for these materials.

Nonetheless, future work on other materials or at low temperatures may require triplet decay to be explicitly addressed. In these circumstances, we identify that eq 3 is readily expandable to include these processes with additional terms, for example,

$$\frac{d[T_1]}{dt} = k_{ISC}[S_1] - (k_{rISC} + k_{PH} + k_{nr})[T_1] \quad (4)$$

and that emissive decay from $^1$CT and $^3$LE can usually be resolved spectrally. Identifying when modifications like eq 4 are necessary may require access to transient absorption,

although comparing fitted values of $k_{rISC}$ fit using eq 3 with $k_{PH}$ + $k_{nr}$ (from the inverse of a measured phosphorescence lifetime) may also suffice when absorption measurements are impractical.

## CONCLUSION

We have shown that fitting of transient photoluminescence experiments with a simplified kinetic model yields reliable values for the relevant rate constants of the TADF process. A key parameter for the photophysical characterization, the reverse intersystem crossing rate constants are determined with values of $k_{rISC}$ = 9.8 × $10^5$ $s^{-1}$ for DPEPO:DDMA-TXO2(13%) and $k_{rISC}$ = 1.93 × $10^6$ $s^{-1}$ for CBP:DPTZ-DBTO2(10%) at room temperature, without the need for additional steady state measurements nor choice of a delayed region for exponential fitting. In addition, the model gives the time dependent populations of the singlet and triplet states, reproduces the activation energy of the rISC process from an Arrhenius plot, and due to its kinetic nature can be readily expanded to include rISC rate distributions and triplet decay. Since $k_{rISC}$ is ultimately more important than $\Delta E_{ST}$ for high performance TADF materials we propose that the presented analysis should become standard for characterizing new TADF materials.

## AUTHOR INFORMATION


### Corresponding Authors

*E-mail: nils.haase@external.merckgroup.com.
*E-mail: andrew.danos@durham.ac.uk.

### ORCID

Andrew Danos: 0000-0002-1752-8675
Wolfgang Brütting: 0000-0001-9895-8281
Andrew P. Monkman: 0000-0002-0784-8640


### Notes

The authors declare no competing financial interest.

## ACKNOWLEDGMENTS


This research was supported by the HyperOLED project from the European Unions's Horizon 2020 research and innovation program under Grant Agreement Number 732013.


## REFERENCES


(1) Adachi, C.; Baldo, M. A.; Thompson, M. E.; Forrest, S. R. Nearly 100% Internal Phosphorescence Efficiency in an Organic Light-Emitting Device. *J. Appl. Phys.* **2001**, *90*, 5048−5051.

(2) Baldo, M. A.; O'brien, D.; You, Y.; Shoustikov, A.; Sibley, S.; Thompson, M.; Forrest, S. R. Highly Efficient Phosphorescent Emission from Organic Electroluminescent Devices. *Nature* **1998**, *395*, 151.

(3) Dias, F. B.; Bourdakos, K. N.; Jankus, V.; Moss, K. C.; Kamtekar, K. T.; Bhalla, V.; Santos, J.; Bryce, M. R.; Monkman, A. P. Triplet Harvesting with 100% Efficiency by Way of Thermally Activated Delayed Fluorescence in Charge Transfer Oled Emitters. *Adv. Mater.* **2013**, *25*, 3707−3714.

(4) Jankus, V.; Data, P.; Graves, D.; McGuinness, C.; Santos, J.; Bryce, M. R.; Dias, F. B.; Monkman, A. P. Highly Efficient Tadf Oleds: How the Emitter−Host Interaction Controls Both the Excited State Species and Electrical Properties of the Devices to Achieve near 100% Triplet Harvesting and High Efficiency. *Adv. Funct. Mater.* **2014**, *24*, 6178−6186.

(5) Kondakov, D.; Pawlik, T.; Hatwar, T.; Spindler, J. Triplet Annihilation Exceeding Spin Statistical Limit in Highly Efficient Fluorescent Organic Light-Emitting Diodes. *J. Appl. Phys.* **2009**, *106*, 124510.

(6) Méhes, G.; Nomura, H.; Zhang, Q.; Nakagawa, T.; Adachi, C. Enhanced Electroluminescence Efficiency in a Spiro-Acridine Derivative through Thermally Activated Delayed Fluorescence. *Angew. Chem., Int. Ed.* **2012**, *51*, 11311−11315.

(7) Sivasubramaniam, V.; Brodkorb, F.; Hanning, S.; Loebl, H. P.; van Elsbergen, V.; Boerner, H.; Scherf, U.; Kreyenschmidt, M. Fluorine Cleavage of the Light Blue Heteroleptic Triplet Emitter Firpic. *J. Fluorine Chem.* **2009**, *130*, 640−649.

(8) Uoyama, H.; Goushi, K.; Shizu, K.; Nomura, H.; Adachi, C. Highly Efficient Organic Light-Emitting Diodes from Delayed Fluorescence. *Nature* **2012**, *492*, 234.

(9) Wang, H.; Xie, L.; Peng, Q.; Meng, L.; Wang, Y.; Yi, Y.; Wang, P. Novel Thermally Activated Delayed Fluorescence Materials−Thioxanthone Derivatives and Their Applications for Highly Efficient Oleds. *Adv. Mater.* **2014**, *26*, 5198−5204.

(10) Etherington, M. K.; Gibson, J.; Higginbotham, H. F.; Penfold, T. J.; Monkman, A. P. Revealing the Spin−Vibronic Coupling Mechanism of Thermally Activated Delayed Fluorescence. *Nat. Commun.* **2016**, *7*, 13680.

(11) Bergmann, L.; Hedley, G. J.; Baumann, T.; Bräse, S.; Samuel, I. D. Direct Observation of Intersystem Crossing in a Thermally Activated Delayed Fluorescence Copper Complex in the Solid State. *Sci. Adv.* **2016**, *2*, No. e1500889.

(12) Kirchhoff, J. R.; Gamache, R. E., Jr; Blaskie, M. W.; Del Paggio, A. A.; Lengel, R. K.; McMillin, D. R. Temperature Dependence of Luminescence from Cu (Nn) 2+ Systems in Fluid Solution. Evidence for the Participation of Two Excited States. *Inorg. Chem.* **1983**, *22*, 2380−2384.

(13) Parker, C.; Hatchard, C. Triplet-Singlet Emission in Fluid Solutions. Phosphorescence of Eosin. *Trans. Faraday Soc.* **1961**, *57*, 1894−1904.

(14) Dias, F. B.; Santos, J.; Graves, D. R.; Data, P.; Nobuyasu, R. S.; Fox, M. A.; Batsanov, A. S.; Palmeira, T.; Berberan-Santos, M. N.; Bryce, M. R.; Monkman, A. P. The Role of Local Triplet Excited States and D-A Relative Orientation in Thermally Activated Delayed Fluorescence: Photophysics and Devices. *Adv. Sci.* **2016**, *3*, 1600080.

(15) Dias, F. B.; Penfold, T. J.; Monkman, A. P. Photophysics of Thermally Activated Delayed Fluorescence Molecules. *Methods Appl. Fluoresc.* **2017**, *5*, 012001.

(16) Gan, L.; Gao, K.; Cai, X.; Chen, D.; Su, S.-J. Achieving Efficient Triplet Exciton Utilization with Large $\Delta E_{st}$ and Non-Obvious Delayed Fluorescence by Adjusting Excited State Energy Levels. *J. Phys. Chem. Lett.* **2018**, *9*, 4725.

(17) Kobayashi, T.; Niwa, A.; Takaki, K.; Haseyama, S.; Nagase, T.; Goushi, K.; Adachi, C.; Naito, H. Contributions of a Higher Triplet Excited State to the Emission Properties of a Thermally Activated Delayed-Fluorescence Emitter. *Phys. Rev. Appl.* **2017**, *7*, 034002.

(18) Kobayashi, T.; Niwa, A.; Haseyama, S.; Takaki, K.; Nagase, T.; Goushi, K.; Adachi, C.; Naito, H. Emission Properties of Thermally Activated Delayed Fluorescence Emitters: Analysis Based on a Four-Level Model Considering a Higher Triplet Excited State. *J. Photonics Energy* **2018**, *8*, 032104.

(19) Penfold, T.; Dias, F.; Monkman, A. The Theory of Thermally Activated Delayed Fluorescence for Organic Light Emitting Diodes. *Chem. Commun.* **2018**, *54*, 3926−3935.

(20) dos Santos, P. L.; Etherington, M. K.; Monkman, A. P. Chemical and Conformational Control of the Energy Gaps Involved in the Thermally Activated Delayed Fluorescence Mechanism. *J. Mater. Chem. C* **2018**, *6*, 4842−4853.

(21) Ogiwara, T.; Wakikawa, Y.; Ikoma, T. Mechanism of Intersystem Crossing of Thermally Activated Delayed Fluorescence Molecules. *J. Phys. Chem. A* **2015**, *119*, 3415−3418.
(22) Gibson, J.; Monkman, A. P.; Penfold, T. J. The Importance of Vibronic Coupling for Efficient Reverse Intersystem Crossing in Thermally Activated Delayed Fluorescence Molecules. *ChemPhysChem* **2016**, *17*, 2956−2961.
(23) Marian, C. M. Mechanism of the Triplet-to-Singlet Upconversion in the Assistant Dopant Acrxtn. *J. Phys. Chem. C* **2016**, *120*, 3715−3721.
(24) Ward, J. S.; Nobuyasu, R. S.; Batsanov, A. S.; Data, P.; Monkman, A. P.; Dias, F. B.; Bryce, M. R. The Interplay of Thermally Activated Delayed Fluorescence (Tadf) and Room Temperature Organic Phosphorescence in Sterically-Constrained Donor−Acceptor Charge-Transfer Molecules. *Chem. Commun.* **2016**, *52*, 2612−2615.
(25) Gibson, J.; Penfold, T. Nonadiabatic Coupling Reduces the Activation Energy in Thermally Activated Delayed Fluorescence. *Phys. Chem. Chem. Phys.* **2017**, *19*, 8428−8434.
(26) dos Santos, P. L.; Ward, J. S.; Bryce, M. R.; Monkman, A. P. Using Guest−Host Interactions to Optimize the Efficiency of Tadf Oleds. *J. Phys. Chem. Lett.* **2016**, *7*, 3341−3346.
(27) Lee, I.; Lee, J. Y. Molecular Design of Deep Blue Fluorescent Emitters with 20% External Quantum Efficiency and Narrow Emission Spectrum. *Org. Electron.* **2016**, *29*, 160−164.